Scientific Research Publishing

World Journal of Engineering and Technology, 2025, 13(3), 440-461
https://www.scirp.org/journal/wjet
ISSN Online: 2331-4249
ISSN Print: 2331-4222

Adaptive Artificial Neural Network (ADALINE) Dynamic Phase Error Estimation Based on the Average Correlation Coefficient

Gabriel Musonda, Charles Lubobya, Ackim Zulu

Department of Electrical Engineering, School of Engineering, University of Zambia, Lusaka, Zambia
Email: musondagabriel50@gmail.com, ackim.zulu@unza.zm, cslubobya@unza.zm

How to cite this paper: Musonda, G., Lubobya, C. and Zulu, A. (2025) Adaptive Artificial Neural Network (ADALINE) Dynamic Phase Error Estimation Based on the Average Correlation Coefficient. *World Journal of Engineering and Technology*, **13**, 440-461.
https://doi.org/10.4236/wjet.2025.133028

Received: April 30, 2025
Accepted: June 30, 2025
Published: July 3, 2025

Abstract

This paper presents a new anomaly detection scheme based on modified DFT Adaptive Neural Network (ADALINE) for the determination of time skew error and frequency drift in the Phasor Measurement Unit (PMU). The modified DFT/ADALINE algorithm is used to determine time stamp errors and frequency drift errors through the determination of the change in the phase angle in terms of the correlation coefficient. The correlation coefficient, $\delta_{(\varphi 0,\, t)}$ is used to determine the relationship in the change of the phase angle, $\Delta\varphi_0$ with respect to the change in the reporting time, Δt. Further, the correlation coefficient, $\delta_{(\varphi 0,\, f)}$ is used to determine the relationship between the change of the phase angle, $\Delta\varphi_0$ with respect to drift in the grid frequency, Δf. The parallel ADALINE algorithms compute the correlation coefficient in the range −1 to 1 from which values of $\delta \geq 0.8$ represent normal correlation and $\delta \leq 0.799$ represents data anomaly in the grid frequency or the reporting time. ADALINE flags the values for $\delta \leq 0799$ only thereby reducing the memory requirements of the PMU. The results of PMU/ADALINE simulation in MATLAB/Simulink, show a smooth system response around the optimal operating point of 49.85 Hz at the maximum correlation coefficient value of 0.9974. It further shows that the correlation coefficient is above 0.8 for grid frequencies in the 49.55 Hz to 50.45 Hz range, signifying normal control area operating frequencies in accordance with South African Grid System Operation Code. It can also be seen that a drift in frequency produces a corresponding time error signifying the relationship between the time skew error and frequency drift with the phase angle error in the PMU. Correlation coefficient values below 0.8 signify data Anomalies for the grid frequency outliers *i.e.* corresponding to grid frequencies below 49.5 Hz and above 50.5 Hz. In conclusion, our proposed PMU/ADALINE model guarantees enhanced accuracy and precision of measurement devoid of doing a massive process of iteration as it employees deep

learning AI to compute the correlation coefficient signifying the presence of time skew and grid frequency error.

Keywords

DFT, Adaptive Neural Network (ADALINE), Correlation Coefficient, Time Skew Error, Frequency Drift, Phase Angle Error, Phasor Measurement Unit (PMU)

1. Introduction

Phasor Measurement Technology has established itself among the best Intelligent Electronic Devices (IEDs) for monitoring, protection and control in the power system. In power systems where Phasor Measurement Technology is deployed, it has been established that the external clock signal from the Global Positioning System (GPS) controls timing synchronization of sampled values (SV) and maintains the Total Vector Error (TVE) below the 1% threshold [1]. The internal clock of the Phasor Measurement Unit (PMU) is disciplined by the GPS signal to ensure accuracy in the sampled values and phase angle estimation. As such, issues relating to the accuracy of reported time stamps are among the most difficult to detect and address in Phasor Measurement Technology [2]. In modern power systems, a data processing algorithm, known as the state estimator, is used to convert redundant measurement data into an accurate estimate of the power grid system. The state estimator works perfectly in the Supervisory Control and Data Acquisition (SCADA); a system that is both asynchronous and has a low update rate. In Wide Area Monitoring, Protection and Control (WAMPAC) systems that are synchronous and have high update rates, the state estimator falls short of providing accurate SVs. Even small phase shifts can downgrade the performance of the state estimator, which is an indication of its inability to effectively improve the performance of the PMU [3]. GPS is the most popular choice for the time synchronization problem as it provides sub 100 nanosecond accuracies, and is often used where precision time and frequency synchronization is critical [4]. In PMUs where GPS is used, the Universal Time Reference (UTC) is applied to time stamp the signal. The phase difference between the UTC reference unit and the sinusoid is used as the mark of the stamp. A positive phase angle is obtained if the UTC reference is after the peak sinusoid and a negative phase angle is obtained if the UTC reference mark is before the peak sinusoid [5]. Synchronization issues between different PMU devices result from discrepancies in their internal clocks and their disciplining, that are responsible for generating time stamps for the data [6]. Therefore, alternative sources of time synchronization to the PMU must conform to the standard set by the GPS.

The Total Vector Error (TVE) provides a measurement standard for the SVs that can be used to determine the suitability of the time synchronization source.

It is a measure of steady-state amplitude and phase angle errors. The total vector error (TVE) combines both magnitude and phase errors since the synchrophasor measurement errors could be originated from inaccuracy of either the magnitude, phase, or both [7]. One-cycle Discrete Fourier Transform (DFT) is usually applied in algorithms that are used to determine the TVE. The DFT algorithm usually has issues when it is used to estimate TVE of signals with dynamic amplitude and phase variations [8]. DFT is not robust enough when it encounters certain disturbances such as decaying DC offset. These disturbances can cause undesirable oscillations and time delay in the DFT results [9]. In cases where the frequency of the power grid deviates from its nominal value, the raw application of the DFT approach can lead to large errors during phasor estimation [10]. Numerous improvements of the DFT algorithm have been developed to correct the problem of frequency spectrum deviation over the years. They include Recursive Discrete Fourier Transform (RDFT), and Non-Recursive Discrete Fourier Transform (NRDFT) [11]. Non-DFT algorithms have equally been presented in research involving PMUs; they include the full Weighted Least Square (WLS) technique [12], the Precision Time Protocol (PTP) [13], and the Three-Phase Enhanced Phase-Locked Loop (EPLL) [10]. Anomaly Detection techniques such as the Long Short-Term Memory (LSTM) [14], Convolution Neural Networks (CNN) [15], and the Generative Adversarial Networks (GANs) [16] have equally been presented in literature to correct errors in dynamic phasor estimation. The Non-DFT algorithms were designed to enhance accuracy and precision of measurement devoid of doing a massive process of iteration. In this paper, section 1 carries the introduction of the work presented. In section 2, basic phasor equations are presented to explain the time skew error concept. In section 3, a hybrid AI based anomaly detection and Phase-locked loop architecture for the PMU is presented. In section 4, performance evaluation of the PMU prototype using real time measurement data is presented. The conclusion of the work is presented in section 5.

2. Related Work

Anomaly detection techniques using artificial intelligence (AI) have been deployed in a number of electrical engineering related works. Mohammed Q. Mohammed *et al.* [17], used single-class Support Vector Machine (SVM) to detect data anomalies in wireless networks. The results show that SVM properly detected and mitigated cybersecurity risks in wireless networks with a precision value of 0.0922.

Shiyuan Wang *et al.*, [18] used Artificial Neural Network (ANN) to investigate detection and classification, and adaptive condition-awareness high-fidelity measurements in real-time transient stability analysis (TSA). The results show the scheme produced classification accuracy on multiple classes of prevailing conditions in the power grid which accordingly improves the measurement quality and attains promising performance when employed in power system applications using synchrophasor measurements.

Yuval Abraham Regev *et al.* [19] deployed Long Short Term Memory (LSTM) and Convolutional Neural Network (CNN) to investigate data anomalies in the PMU caused by physical faults on the power grid, as well as disturbances, errors, and cyber-attacks in the cyber area. The investigation was conducted by training the PMU model using Mean Squared Error (MSE) that heavily punishes the outliers in the data set. The results of this investigation show satisfactory results in the range of 78.79% to 96.89%.

Watit Benjapolakul *et al.* [20] proposed the development of a PMU prototype based on the Bagged Averaging of Multiple Linear Regression model, which handles and fulfills the missing values in synchronized frequency data measurement fast and efficiently. The results show that the model was able to recover missing PMUs data that is acceptable for many real-time applications and to interpret the effects of different grid regions to an event using PMUs data.

This research proposes the application of Adaptive Artificial Neural Network (ADALINE) in the PMU to determine the numerical relationship between time skew error and vector frequency drift, and phase angle error using the correlation coefficient. A ADALINE Time and Frequency Algorithm is applied to determine; the relationship between time skew error and the phase angle error, and also the relationship between the input vector frequency drift and the phase angle error. The results show that the model is able to punish frequency outliers, input vector phase errors above 50˚, all through maintaining a correlation coefficient of 0.8 and above.

3. Literature Review

The time skew error is caused by error in the GPS signal or drift in the input vector frequency and results in phase angle error in the vector output of the PMU. The output of the PMU is called a synchrophasor. The synchrophasor is defined as "a phasor calculated from data samples using a standard time signal as the reference for the measurement" [21]. The GPS provides the reference time signal required in the creation of a synchrophasor by the PMU.

A. Synchrophasor Determination

The phasor can be represented as either a sine or a cosine function as shown below

$$z(t) = Z_m \sin(\omega t + \varphi_0) \tag{1}$$

where Z_m is the amplitude of the signal $z(t)$, ω is the angular velocity ($= 2\pi f$, where f is the frequency), and φ_0 is the phase angle compared with $z(t) = Z_m \sin \omega t$.

$$z(t) = Z_m \cos(\omega t + \varphi_0) \tag{2}$$

It is quite complicated to analyze quantities in the time domain form of Equation (1) and Equation (2). Therefore, an alternative method of representing the function is presented below. This method of synchrophasor presentation is called the Euler's formula.

$$Z_m e^{j(\omega t+\varphi_0)} = Z_m\left(\cos\omega t+\varphi_0\right)+ jZ_m\left(\sin\omega t+\varphi_0\right) = X_r + jX_i \tag{3}$$

Equation (3) presents the phasor signal in terms of the real and imaginary parts denoted as $X_r + jX_i$. Thus a sinusoidal varying signal such as in Equation (1) or Equation (2) can be considered to be either the real or the imaginary part of $Z_m e^{j(\omega t+\varphi_0)}$, depending on whether the cosine or sine function is being considered.

$$Z_m e^{j(\omega t+\varphi_0)} = Z_m e^{j\omega t} e^{j\varphi_0} = phasor \tag{4}$$

Since, the angular velocity is the same for all the elements in a circuit, thus a synchropasor can be described by the equation below

$$Z_m \angle \varphi_0 \tag{5}$$

The exponential form of the cosine function. *i.e.* $z(t) = Z_m \cos(\omega t+\varphi_0)$, can then be described by the equation below

$$z(t) = Z_m\left[\frac{1}{2}\left(e^{j(\omega t+\varphi_0)} + e^{-j(\omega t+\varphi_0}\right)\right]$$

$$z(t) = \frac{1}{2}Z_m e^{j(\omega t+\varphi_0)} + \frac{1}{2}Z_m e^{-j(\omega t+\varphi_0)} \tag{6}$$

Thus $z(t)$ is the sum of two phasors, each with half the amplitude, with one having a positive value of angular velocity (*i.e.* rotating anticlockwise) and a positive value of φ_0, and the other having a negative value of angular velocity and a negative value of φ_0 [22]. It is safe to conclude from this result that $Z_m e^{j(\omega t+\varphi_0)}$ is the fundamental signal while $\frac{1}{2}Z_m e^{j(\omega t+\varphi_0)}$ and $\frac{1}{2}Z_m e^{-j(\omega t+\varphi_0)}$ are the harmonics. This result shows that if the phase shift is associated only to a lack of time synchronization, it is possible to convert a negative phase angle measurement to a positive phase angle measurement by analyzing the signal harmonics. The value of phase angle φ_0 depends on the time scale, at the time instant of $t = 0$. Provided that the definition of the above phasor is based on the angular frequency ω, the elaboration with other phasors must be realized with the same frequency and time instant [23].

The phase angle φ_0 is the difference between the instantaneous phase angle of $z(t)$ and a reference cosine signal running at the nominal frequency of the grid aligned to Coordinated Universal Time (UTC) [24]. This phase angle φ_0 can assume a positive value if the UTC reference is after the pick sinusoid of the signal. Negative value is obtained when the UTC reference is before the pick sinusoid of the signal.

For analysis of signals with dynamic amplitude and phase variations, the signal in Equation (2) can be written as

$$z(t) = Z_m \cos\left(2\pi f_0 t + 2\pi\int a(t)\mathrm{d}t + \varphi_0\right) \tag{7}$$

Where;

$$a(t) = f(t) - f_0$$

where f_0 and $f(t)$ are the nominal and the actual frequency, respectively, and

$a(t)$ is the function of time that indicates the deviation of the actual from the nominal frequency. For a fixed frequency deviation, the input signal of Equation (7) can be represented by Equation (8) below

$$z(t) = Z_m \cos\left(\left(2\pi f_0 + 2\pi\Delta f\right)t + \varphi_0\right) \tag{8}$$

where $f + \Delta f$ is the off-nominal frequency and Δf represents the fixed frequency deviation.

B. Synchrophasor Determination Using DFT

In a balanced three-phase system operating at a nominal frequency, f_0 the signal waveforms can be represented by the equations below

$$z(t) = Z_m \cos\left(2\pi f_0 t + \varphi_0\right) \tag{9}$$

The time domain sample of the signal in Equation (9) can be represented by;

$$z_n = Z_m \cos\left(\frac{2\pi n}{N} + \varphi_0\right) \tag{10}$$

where N is the number of samples and is an integer multiple of fundamental frequency f_0 and n represents the sample index in the array which ranges from 0 to $N-1$ [25].

For N number of samples, the expression below applies

$$Z = \frac{1}{N}\sum_{n-0}^{N-1} z_n\left(\cos\frac{2\pi n}{N} - j\sin\frac{2\pi n}{N}\right) \tag{11}$$

The Discrete Fourier Transform (DFT) of the signal can be determined by the equation

$$Z_{nominal} = \frac{\sqrt{2}}{N}\sum_{n-0}^{N-1} z_n\left(\cos\frac{2\pi n}{N} - j\sin\frac{2\pi n}{N}\right) \tag{13}$$

In this case, the real and imaginary part of the expression can be given by the expressions below

$$Z_{real} = \frac{\sqrt{2}}{N}\sum_{n-0}^{N-1} z_n\left(\cos\frac{2\pi n}{N}\right) \tag{14}$$

$$Z_{imaginary} = \frac{\sqrt{2}}{N}\sum_{n-0}^{N-1} z_n\left(\sin\frac{2\pi n}{N}\right) \tag{15}$$

For the off-nominal frequency signal of Equation (8) above, the time domain sample can be represented by

$$z_n = Z_m \cos\left(2\pi f_0 T_s + 2\pi\Delta f T_s + \varphi_0\right) \tag{16}$$

where z_n are the samples taken in one window with length of NT_s, $(n = 0,1,2,\cdots,N-1)$ [26].

C. Detection of Time Skew Error Using AI

The discrete Fourier transform (DFT) estimation technique is the basic, simplest, and most popular algorithm for phasor computation [27]. In DFT-PMUs Time-skew error is normally determined in terms of phase-angle error. In modern power systems where abnormal conditions arise from the injection of renewal en-

ergy into the grid, off-nominal frequency conditions circumstances lead to serious positive-phase sequence measurement errors. In [28], the Phase-locked loop (PLL) is used to determine the performance analysis of the PMU under grid fault conditions. The PLL configuration shown in **Figure 1** below treats the phase angle error as a data anomaly. The phase detector calculates the time-phase angle difference between the input signal and the output signal. The error signal becomes the input to the LPF to determine the stability and the overall response of the system.

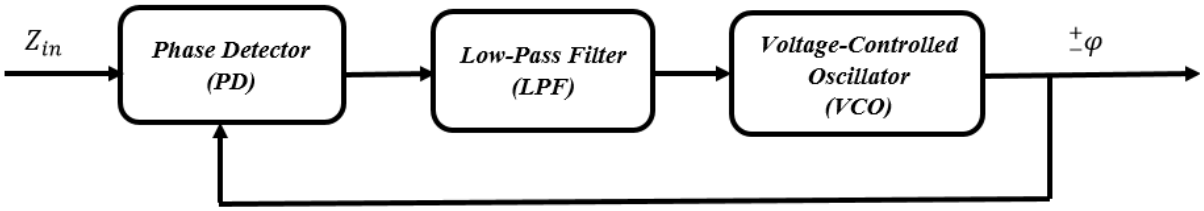

Figure 1. Single-phase Phase-Locked Loop (PLL) block diagram.

This technique, however, suffers from inaccuracies under grid voltage harmonics, inter-harmonics and DC-offset [29]. To mitigate this problem, Koteswara Rao *et al.* [30] proposed the use of a combined amplitude and phase modulated signal model to approximate frequency ramp, sudden change in amplitude and phase in terms of amplitude and phase modulation signal for a small interval of time using feed forward Artificial Neural Network (ANN). ANN process inputs via linear combinations of weights and biases while biological neurons (dynamic) exhibit more dynamic and nonlinear behaviors [31]. ANN suffers from high computational complexity and hardware implementation. A modified Gauss-Newton ADALINE (MGNA) that uses recursive formulation and reduces the computational burden is proposed in [32]. It comes with the promise of determining the fundamental and harmonic phasors while maintaining simple hardware implementation and computation complexity. ADALINE is a linear AI algorithm that can be implemented in multiple arrays, called MADALINE to deal with non-linear grid conditions. The MADALINE concept is adopted in this research.

4. Hypothesis and Algorithms

Our hypothesis is that if a GPS signal error or frequency error occurs in the electric grid, the PMU will detect the change in the dynamic conditions to ascertain the correlation of these grid conditions with the phase angle change in the measured vector signal. There are correlations in a single change of a grid parameter or multiple changes in different grid parameters to the phase angle error that can be investigated using ADALINE AI. To investigate these correlations, the linear product correlation coefficient formula is used:

$$r = \frac{\sum(x_i - \bar{x})\sum(y_i - \bar{y})}{\sqrt{\sum(x_i - \bar{x})^2 \sum(y_i - \bar{y})^2}}$$

where r is an indicator of how well the points (x_i, y_i) fit a straight line [33]. r is a number between −1 and 1. In this work, r is used a measure the correlation between the change in the input vector frequency and the change in the measured vector phase angle on one hand; and the error in the time stamp to the change in the measured vector phase angle by the PMU on the other hand. The computation complexity is reduced by the application of the ADALINE.

For a fixed frequency deviation, the phasor signal can be represented by the equation below

$$z(t) = Z_m \cos\left(\left(2\pi f_0 + 2\pi\Delta f\right)t + \varphi_0\right) \tag{17}$$

where $f_0 + \Delta f$ is the off-nominal frequency and Δf represents the fixed frequency deviation. The phase angle deviation φ_0 from a time t_1 to t_2 can be derived from Equation (18) below

$$\varphi_0 = 2\pi\int_{t_1}^{t_2}\left[\Delta f - f_0\right]\mathrm{d}t \tag{18}$$

And the relative phase angle can be measured from Equation (19) below

$$\varphi_{rel} = \varphi_0 - \varphi_{ref} \tag{19}$$

where φ_0 is the measured phase angle and φ_{ref} is the phase angle of the reference PMU. The PMU reporting time Δt can be represented by the equation

$$\Delta t = t_2 - t_1 \tag{20}$$

Therefore, the variation of the relative phase angle will be given by Equation (21) below

$$\Delta\varphi_{rel} = \Delta\varphi_0 - \Delta\varphi_{ref} \tag{21}$$

Further, the change in relative phase angle can represented by Equation (22) below

$$\Delta\varphi_0 = 2\pi\int_{t_2-\Delta t}^{t_2}\left[\Delta f - f_0\right]\mathrm{d}t \tag{22}$$

In the event of time skew error in the PMU, the inaccurate time t_s is defined by the expression below

$$t_s = t + \tau \tag{23}$$

where t_s is the shift in UTC time, t is the UTC reference time, and τ is the deviation from the UTC time.

$$\Delta\varphi_0\left(t_s\right) = \Delta\varphi_{rel}\left(t\right) + 2\pi\cdot\Delta f_\tau\left(t\right)\Delta t \tag{24}$$

Equation (24) is used to detect anomalies in the timestamps of the synchrophasor. Where $\Delta\varphi_0\left(t_s\right)$ is the variation of relative phase angle with timestamp shifting, $f\left(t\right)$ denotes the instant frequency of measured signal at the time t and $\Delta f_\tau\left(t\right)$ is frequency variation between time t_s and t [34]. The outputs of the PMU are fed to the ADALINE to compute the correlation coefficient to be used for determination of normal and abnormal grid conditions as illustrated in **Figure 2** below.

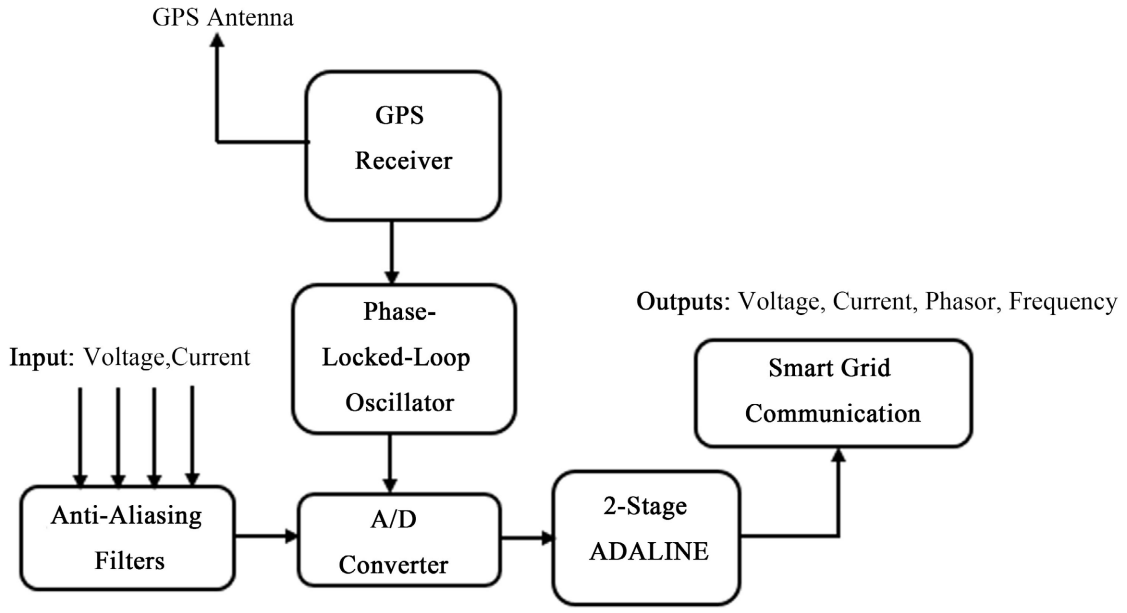

Figure 2. AI Based PMU Block diagram.

For single input ADALINE, one variable one output scenario, Equation (25) will be used to determine the phase angle error with respect to the shift in the time stamp *i.e.* time stamp shifting condition.

$$\Delta\varphi_0(t_s) = \Delta\varphi_{rel}(t) + 2\pi f \Delta t \tag{25}$$

The time skew error is simulated by inducing a shift in time τ as a function of the drift in the input vector frequency. The adaptive linear neuron (ADALINE) computes the correlation coefficient for this condition.

It can be observed that t_s can be updated iteratively. The formulations for updating the time shift by substituting the relative change in UTC time Δt in (25) is as shown below

$$\begin{aligned} t_s(n+1) &= t + \Delta\tau \\ t_s(n+2) &= t + 2\Delta\tau \\ t_s(n+3) &= t + 3\Delta\tau \\ t_s(n+4) &= t + 4\Delta\tau \\ t_s(n+\cdots) &= t + (n+\cdots)\Delta\tau \end{aligned} \tag{26}$$

To determine the correlation between the change in the phase angle and the shift in the time, the equation below is used [34].

$$\delta_{(\varphi_0,t)} = \frac{\sigma_{(\varphi_0,t)}}{\sigma_{\varphi_0}\sigma_t} \tag{27}$$

where r is the correlation factor, $\sigma_{(\varphi_0,t)}$ is the covariance, σ_{φ_0} and σ_t are the phase angle and time respective standard deviations. These parameters are defined in the equations below

$$\delta_{(\varphi_0,t)} = \frac{\sum\left(\varphi_0 - \varphi_{ref}\right)\left(t_2 - t_1\right)}{\sqrt{\sum\left(\varphi_0 - \varphi_{ref}\right)^2 \sum\left(t_2 - t_1\right)^2}} \tag{28}$$

The correlation coefficient will be used to ascertain how the phase angle φ_0 correlates with the time t. $\delta_{(\varphi_0,t)} \geq 0.8$, represents normal grid conditions *i.e.* phase angle φ_0 and the time t. Since the equation for the determination of the change in the phase angle $\Delta\varphi_0\left(t_s\right)$ is linear, $\delta_{(\varphi_0,t)} \leq 0.799$ represents the lack of correlation between the variables. In this work, $\delta_{(\varphi_0,t)} \leq 0.799$ is treated as a data anomaly.

For single input ADALINE, one variable one output scenario, Equation (29) will be used to determine the phase angle change with variable frequency *i.e.* frequency shifting condition.

$$\Delta\varphi_0\left(f_s\right) = \Delta\varphi_{rel}\left(t\right) + 2\pi \cdot \Delta f_\tau\left(t\right)t \tag{29}$$

The frequency drift error is simulated by inducing a shift in frequency. $\Delta f_\tau\left(t\right)$ ranging from −0.55 to 0.55 off the nominal 50 hz frequency. The adaptive linear neuron (ADALINE) computes the correlation coefficient for this condition.

It can be observed that the frequency, f can be updated iteratively. The formulations for updating the shift in the frequency f by substituting the relative change in frequency Δf in (30) is as shown below

$$\begin{aligned} f_t\left(n+1\right) &= f + \Delta f_\tau \\ f_t\left(n+2\right) &= f + 2\Delta f_\tau \\ f_t\left(n+3\right) &= f + 3\Delta f_\tau \\ f_t\left(n+4\right) &= f + 4\Delta f_\tau \\ f_t\left(n+\cdots\right) &= f + \left(n+\cdots\right)\Delta f_\tau \end{aligned} \tag{30}$$

To determine the correlation between the change in the phase angle and the shift in the frequency, the equation below is used [34]

$$\delta_{(\varphi_0,f)} = \frac{\sigma_{(\varphi_0,f)}}{\sigma_{\varphi_0}\sigma_f} \tag{31}$$

where r is the correlation factor, $\sigma_{(\varphi_0,f)}$ is the covariance, σ_{φ_0} and σ_f are the phase angle and time respective standard deviations. These parameters are defined in the equations below

$$\delta_{(\varphi_0,f)} = \frac{\sum\left(\varphi_0 - \varphi_{ref}\right)\left(f_2 - f\right)}{\sqrt{\sum\left(\varphi_0 - \varphi_{ref}\right)^2 \sum\left(f_2 - f\right)^2}} \tag{32}$$

The correlation coefficient will be used to ascertain how the phase angle φ_0 correlates with the frequency, f. If $\delta_{(\varphi_0,f)} \geq 0.8$ shows normal correlation between the phase angle φ_0 and the frequency, f. Since the equation for the

determination of the change in the phase angle $\Delta\varphi_0(t_s)$ is linear, $\delta_{(\varphi_0,f)} \leq 0.799$ represents the lack of correlation between the variables. In this work, $\delta_{(\varphi_0,f)} \leq 0.799$ is treated as a data anomaly.

5. Methodology

The test signal can be calculated and implemented to distinguish between a real fault situation and a normal operating condition through the computation of the correlation factor for the change in the frequency and the phase angle. The use of ADALINE AI in the configuration utilizes deep learning of the grid operating conditions thereby increasing measurement accuracy and efficiency significantly. This can be implemented in MATLAB/Simulink. In order to calculate the phase-shift, the input signal has to be compared with a reference signal [35]. The computation of the phase-shift will be done by the ADALINE algorithm in the PMU.

To validate the application of the ADALINE in the determination of the correlation coefficient of the frequency drift and time-skew error to the change in the phase angle error, the PMU prototype is simulated in MATLAB/Simulink as shown in Figure 3 below.

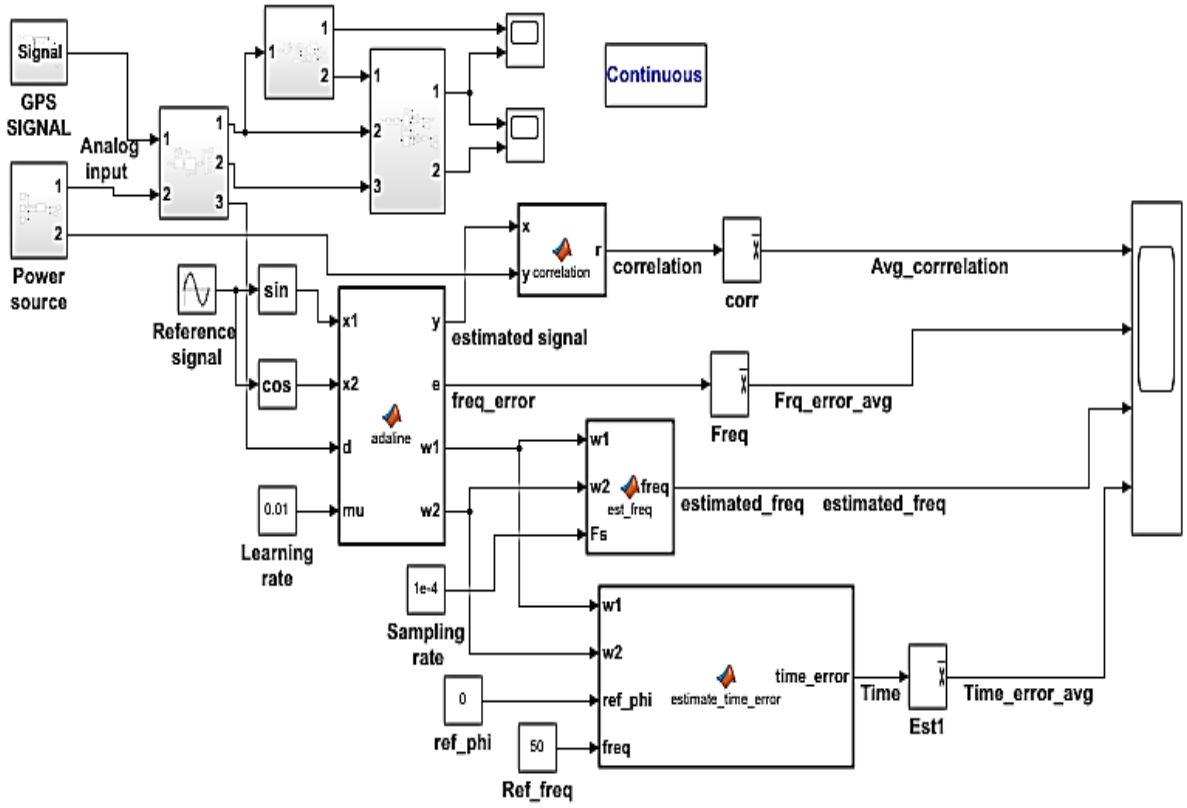

Figure 3. PMU/ADALINE Prototype.

Figure 4 shows the ADALINE configuration in MATLAB/Simulink.

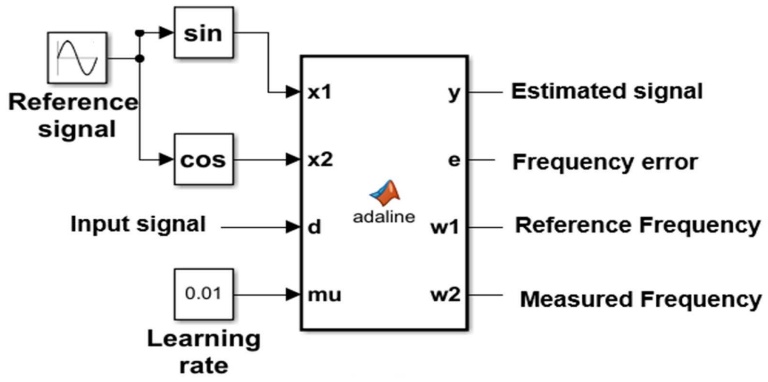

Figure 4. ADALINE Module in simulink.

The PMU/ADALINE prototype is simulated in MATLAB/Simulink for proof of concept. **Figure 5** below shows the algorithm flow chart and frequency error equation.

$$\Delta\varphi_0\left(f_s\right)=\Delta\varphi_{rel}\left(t\right)+2\pi\cdot\Delta f_\tau\left(t\right)t$$

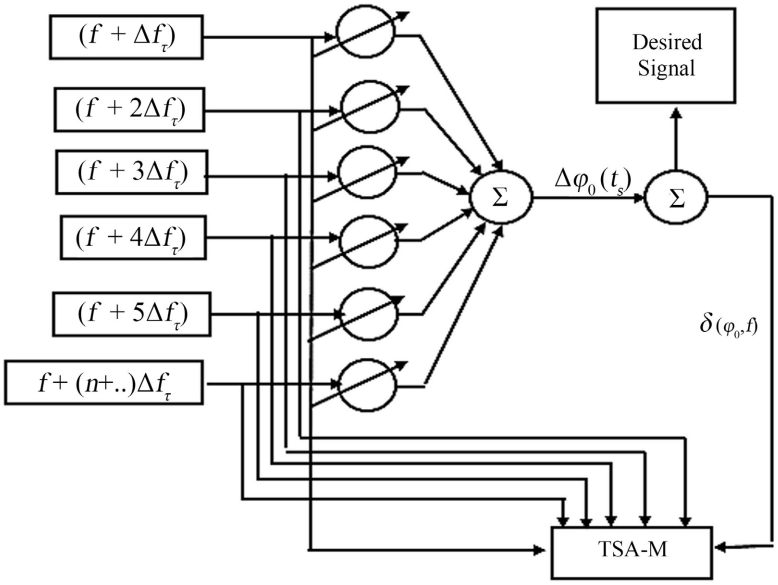

Figure 5. PMU/ADALINE frequency subsystem flow chart.

Step 1. Initialize ADALINE with reference phase angle φ_{ref}, shift in the frequency, Δf_τ with values ranging from −1 to 1hz to estimate the change in phase angle using equation (29).

Step 2. Calculate the correlation factor $\delta_{(\varphi_0,f)}$ using equation (32).

Step 3. Check if correlation factor $\delta_{(\varphi_0,f)}$ exceeds $\delta_{(\varphi_0,f)}\leq 0.799$.

Step 4. Update Δf_τ using (30) until error is achieved.

Step 5. Continue till the maximum number of iterations are reached.

Step 6. End.

Figure 6 below shows the MATLAB/Simulink implementation of the algo-

rithm.

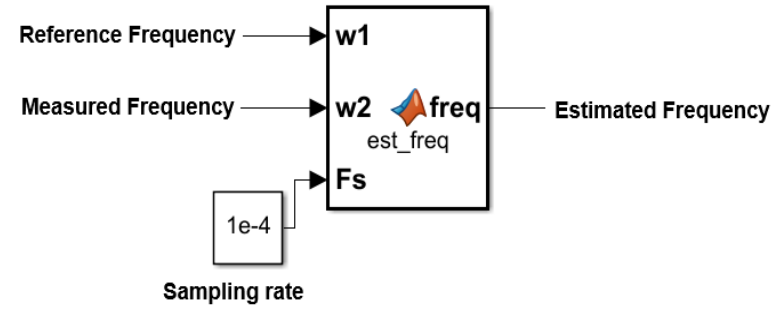

Figure 6. Simulink frequency estimation module.

The PMU/ADALINE prototype is simulated in MATLAB/Simulink for proof of concept. **Figure 7** below shows the algorithm flow chart and time error equation are provided below;

$$\Delta\varphi_0(t_s) = \Delta\varphi_{rel}(t) + 2\pi f \Delta t$$

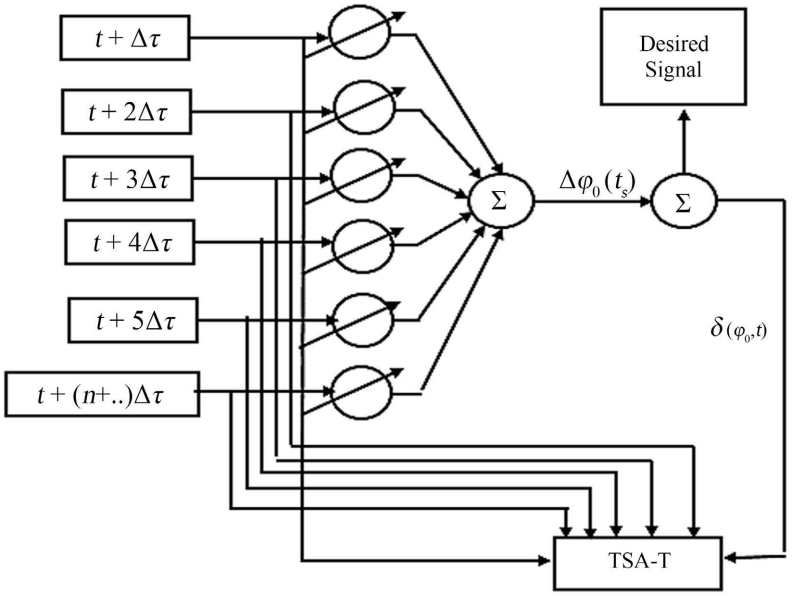

Figure 7. PMU/ADALINE time subsystem flow chart.

Step 1. Initialize ADALINE with reference phase angle φ_{ref}, shift in the UTC, τ with values ranging from 0.1 to 0.2 seconds to estimate the change in phase angle using Equation (26).

Step 2. Calculate the correlation factor $\delta_{(\varphi_0,t)}$ using Equation (28).

Step 3. Check if correlation factor $\delta_{(\varphi_0,t)}$ exceeds $\delta_{(\varphi_0,t)} \le 0.799$.

Step 4. Update $\Delta\tau$ using (24) until error is achieved.

Step 5. Continue till the maximum number of iterations are reached.

Step 6. End.

Figure 8 below shows the MATLAB/Simulink implementation of the algorithm

Figure 8. Simulink time error estimation module.

The correlation coefficient is calculated using the equations below

$$\delta_{(\varphi_0,f)} = \frac{\sum(\varphi_0 - \varphi_{ref})(f_2 - f)}{\sqrt{\sum(\varphi_0 - \varphi_{ref})^2 \sum(f_2 - f)^2}}$$

$$\delta_{(\varphi_0,t)} = \frac{\sum(\varphi_0 - \varphi_{ref})(t_2 - t_1)}{\sqrt{\sum(\varphi_0 - \varphi_{ref})^2 \sum(t_2 - t_1)^2}}$$

Figure 9 below shows the MATLAB/Simulink implementation of the correlation coefficient computations.

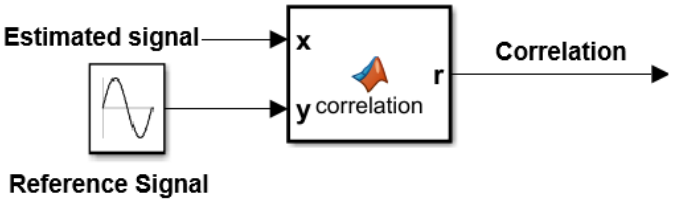

Figure 9. Simulink correlation coefficient estimation module.

6. Results and Discussion

The completeness of the hypothesis of using the correlation coefficient to determine data anomalies in the form grid frequency drift and Time Skew Error was confirmed by the simulation of the model in MATLAB/Simulink. The PMU/ADALINE error computation rate is 0.006 seconds was used in the simulations. The simulation results are presented in Table 1.

The graph shows a semi-parabolic curve. Average correlation at 49.45 Hz is low at approximately 0.75, increases steadily reaching its peak values in the range 49.80 - 49.85 Hz at the maximum correlation coefficient value of 0.9974. Beyond the 0.9974 peak value, the correlation coefficient steadily declines to 0.7535 at 50.55 Hz. The graph is symmetric around the 0.9974 peak value; signifying a smooth system response around the optimal operating point. The highest correlation zone lies Approximately between 0.996 and 0.997, and covers a narrow band centered just below the 50 Hz threshold; representing the most reliable region for the system. Outside the 50.30 to 49.60 Hz zone, the correlation reduces more rapidly, indicating a fall-off in system performance.

Table 1. Correlation coefficient analysis of the input vector frequency error.

Input Vector Freq.	Mea. Ref. Time (UTC)	Time Err. Avg.	Freq. Error Avg.	Avg. Corr.
49.45	0.795	4.485e−4	3.584e−1	7.522e−1
49.50	0.795	6.416e−4	4.101e−1	7.899e−1
49.55	0.795	7.735e−4	4.442e−1	8.608e−1
49.60	0.795	8.520e−4	4.588e−1	9.535e−1
49.65	0.795	8.833e−4	4.528e−1	9.892e−1
49.70	0.795	8.719e−4	4.268e−1	9.956e−1
49.75	0.795	8.200e−4	3.824e−1	9.972e−1
49.80	0.795	7.290e−4	3.222e−1	9.974e−1
49.85	0.795	5.991e−4	2.500e−1	9.972e−1
49.90	0.795	4.315e−4	1.703e−1	9.971e−1
49.95	0.795	2.290e−4	8.797e−2	9.969e−1
50.00	0.795	−1.965e−6	8.060e−3	9.964e−1
50.05	0.795	−2.512e−4	−6.452e−2	9.954e−1
50.10	0.795	−5.408e−4	−1.253e−1	9.935e−1
50.15	0.795	−7.478e−4	−1.708e−1	9.905e−1
50.20	0.795	−9.657e−4	−1.976e−1	9.850e−1
50.25	0.795	−1.146e−3	−2.047e−1	9.733e−1
50.30	0.795	−1.279e−3	−1.915e−1	9.461e−1
50.35	0.795	−1.354e−3	−1.588e−1	9.014e−1
50.40	0.795	−1.358e−3	−1.086e−1	8.542e−1
50.45	0.795	−1.267e−3	−4.413e−2	8.128e−1
50.50	0.795	−1.045e−3	3.075e−2	7.790e−1
50.55	0.795	−6.783e−4	1.114e−1	7.535e−1

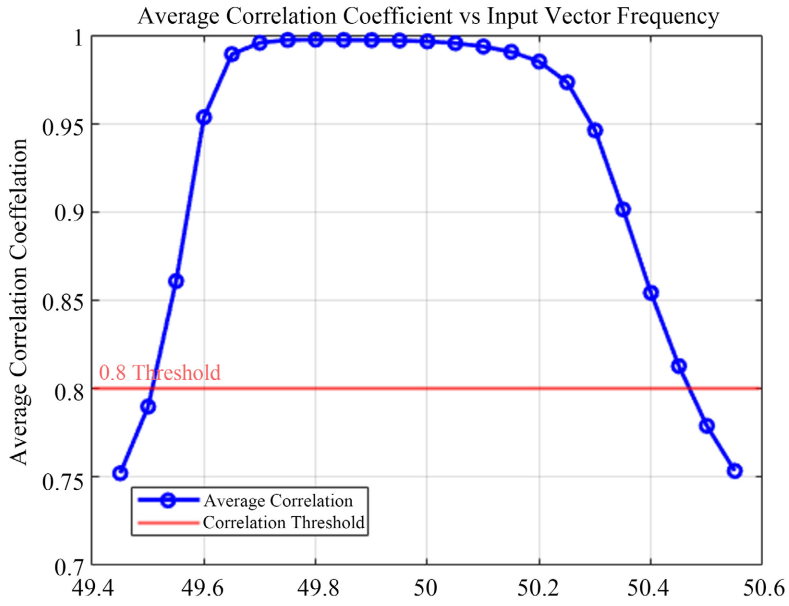

Figure 10. Input vector frequency vs. average correlation coefficient.

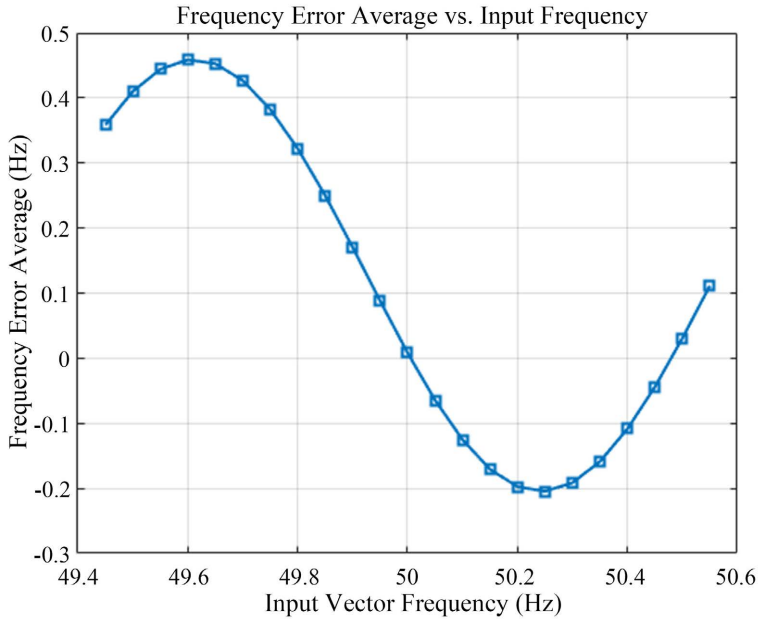

Figure 11. Input vector frequency vs. frequency error average.

The graph shows a clear nonlinear diminishing trend. At 49.45 Hz, the frequency error at approx. 0.3584 Hz is large and positive depicting weak correlation with the input frequency. The frequency error gradually decreases, as the input frequency increases, crossing zero mark at 50.00 Hz. Beyond the 50.00 Hz mark, the error becomes negative, reaching a minimum slightly 50.20 Hz mark, crossing the zero mark again after the 50.45 Hz point.

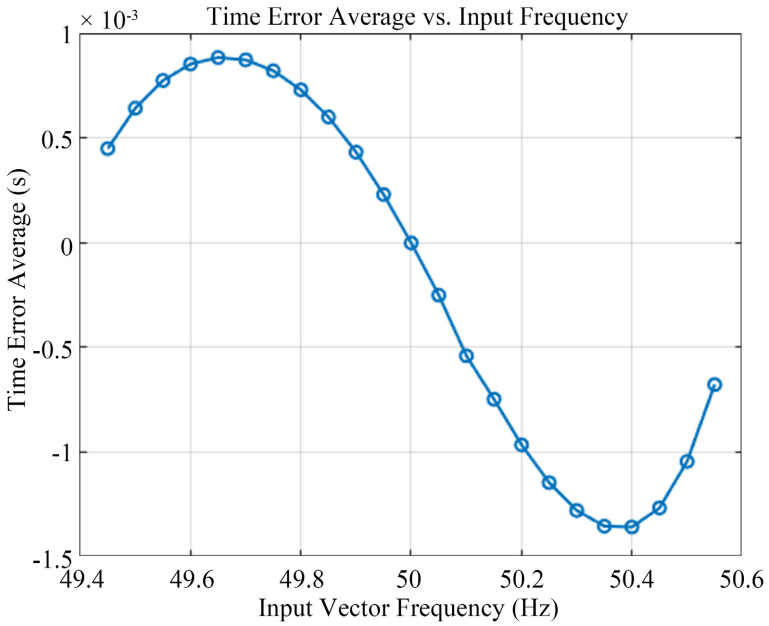

Figure 12. Input vector frequency vs. time error average.

The graph shows a non-linear decreasing movement from 49.45 Hz to about 49.70

Hz. The time error increases steadily, peaking around 8.833e−4 seconds. Beyond the 49.70 Hz point, the time error progressively decreases, crossing zero at approx. 50.00 Hz. At the 50.00 Hz point and beyond, the time error is increasingly negative, reaching a minimum between 50.35 Hz and 50.40 Hz. The curve levels slightly after the minimum point, indicating the error is approaching a steady lower limit (Table 2).

Table 2. Correlation coefficient analysis of the input vector phase angle.

Input Vector Freq.	Mea. Ref. Time (UTC)	Input Vector Phase Angle θ°	Time Err. Avg. θ°	Freq. Error Avg. θ°	Avg. Corr. θ°
50.00	0.795	5	−1.268e−2	−1.259e−2	9.978e−1
50.00	0.795	10	−2.573e−4	−2.224e−2	9.964e−1
50.00	0.795	15	−3.881e−4	−2.997e−2	9.908e−1
50.00	0.795	20	−5.188e−4	−3.569e−2	9.800e−1
50.00	0.795	25	−6.484e−4	−3.938e−2	9.630e−1
50.00	0.795	30	−7.764e−4	−4.101e−2	9.396e−1
50.00	0.795	35	−9.020e−4	−4.056e−2	9.103e−1
50.00	0.795	40	−1.025e−3	−3.803e−2	8.762e−1
50.00	0.795	45	−1.143e−3	−3.385e−2	8.387e−1
50.00	0.795	50	−1.258e−3	−2.685e−2	7.994e−1
50.00	0.795	55	−1.368e−3	−1.828e−2	7.597e−1
50.00	0.795	60	−1.472e−3	7.807e−3	7.206e−1
50.00	0.795	65	−1.570e−3	4.492e−3	6.828e−1
50.00	0.795	70	−1.662e−3	1.852e−2	6.468e−1
50.00	0.795	75	−1.746e−3	3.418e−2	6.128e−1
50.00	0.795	80	−1.824e−3	5.134e−2	5.808e−1
50.00	0.795	85	−1.853e−3	6.987e−2	5.509e−1
50.00	0.795	90	−1.954e−3	8.964e−2	5.320e−1

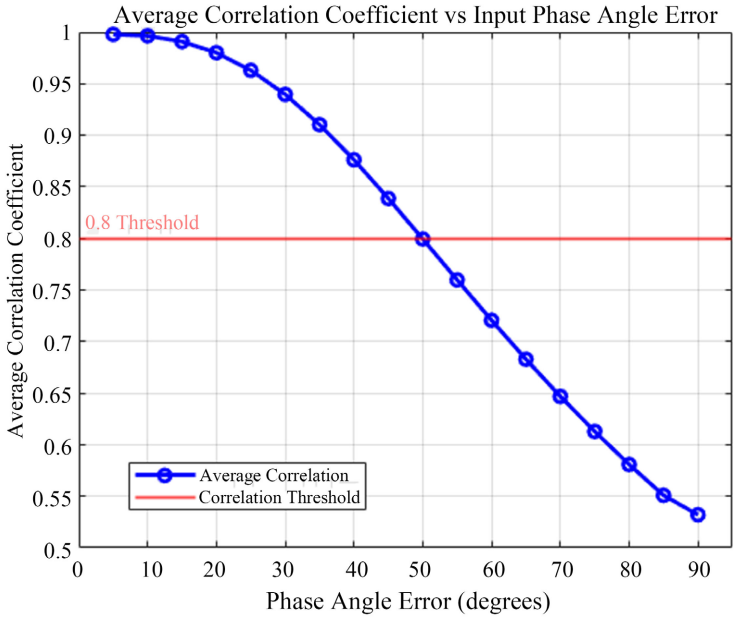

Figure 13. Phase angle error vs average correlation coefficient.

The curve shows a strong decreasing trend in the Average Correlation Coefficient as the phase angle error increases from 5˚ to 90˚. The average correlation value is above 0.9 with the peak at 0.9978. The region between the 45˚ and 50˚ range indicates the point at which the curves cross the 0.8 threshold. The average correlation value rapidly drops below 0.7 at 65˚ and finally to 0.532 at 90˚. The curve depicts a very strong negative correlation between the phase angle error and the average correlation.

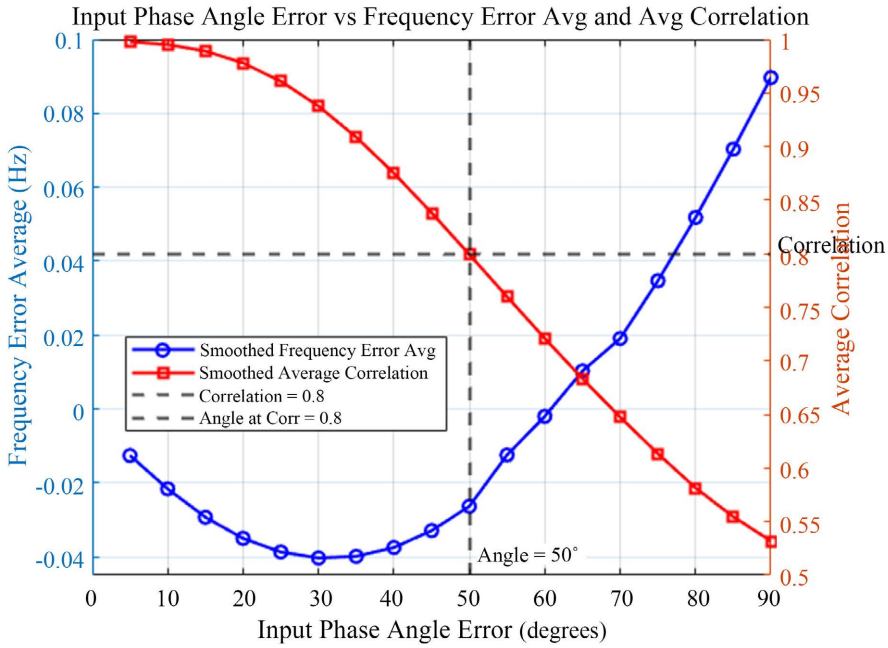

Figure 14. Input phase angle error vs. average correlation/frequency error average.

Frequency Error Average largely decreases as the input phase angle rises up to the 50˚ point; it then sharply begins to rise. The graph shows a consistent and uninterrupted decrease in the Average Correlation with increasing phase angle error. Low phase errors (0˚ to 50˚) correspond with correlation values of 0.8 and above which is consistent with the hypothesis of this research. The PMU/ADALINE algorithm demonstrates that it is highly phase-sensitive, maintains frequency tracking and correlation beyond a certain error margin.

7. Conclusions

The input vector frequency versus frequency error average graph represents a correction curve, where the frequency error is high when the input deviates from a nominal frequency value of 50 Hz. The shape of the curve suggests a slightly asymmetric parabolic profile which indicates non-linear behavior in the system.

The input vector frequency versus time error average curve suggests that the system's timing error is frequency-dependent, with optimal performance at 50.00 Hz**.** The peak in time error occurs at approximately 49.65 Hz and valley at approximately 50.35 Hz indicating system lag or phase shift on either side of the

nominal frequency.

The input vector frequency versus average correlation curve reflects the quality of signal matching, orientation, and model precision at different input frequencies. The peak in correlation implies that the system is optimized for a specific frequency range, centered around 49.80 to 49.90 Hz. As frequency drifts away from this peak range, phase angle error is likely to increase, lowering the correlation. Best system performance for the PMU/ADALINE is dependent on keeping the input vector frequency in the range of 49.65 Hz to 50.05 Hz where the correlation coefficient is greater than 0.99. The region between 49.55 Hz to 49.65 Hz, and 50.05 Hz to 50.45 Hz represents the region where system calibration of correction is considered to be normal. Finally, the correlation coefficient values below 0.799 corresponding to frequencies outside 49.55 Hz and 50.45 Hz are scientifically called data anomalies as they fall outside the acceptable correlation. Outliers, missing data, and event data in the synchrophasor are considered to be data anomalies [36].

In this paper, we have investigated the PMU/ADALINE that works on the principle of computing the correlation coefficient using AI to determine data anomalies of the normal grid operating conditions in a given control area. The control area is considered to be under normal frequency conditions when the frequency is within the range 49.5 to 50.5 Hz [37]. The graph in **Figure 10** shows how the average correlation coefficient changes with the input vector frequency. You can see a clear transition around 49.55 - 50.45 Hz, where the correlation coefficient shifts from $\delta_{(\varphi_0, f)} \leq 0.799$ to $\delta_{(\varphi_0, f)} \geq 0.8$ and then back down again, suggesting a peak correlation around 49.75Hz to 49.85Hz. Further, the graph in **Figure 13** suggests that phase angle error significantly affects the average correlation in a manner similar to the graph in **Figure 10**. The characteristics depicted in both **Figures 10-13** confirm that there is a very strong relationship between the input vector frequency, time error average, the phase angle error and the correlation coefficient.

For optimal performance, analysis of the graph in **Figure 14** suggests that ideally the input vector phase angle error should be less than 50˚. The correlation coefficient is unstable and the frequency error average is high for input vector phase angles above 50˚, which is an indication of loss of coherence. The system behavior indicates that phase error correction beyond the 50˚ threshold is necessary. The results of the MATLAB/Simulink prototype confirm the hypothesis of this research.

Performance analysis of average correlation as a performance parameter can be benefited from further investigation of the systems response to transient conditions, such as thunderstorms and other sources of noise. An inclusion of mathematical analysis of the computation load in DFT PMUs compared to the ADALINE PMU would enrich the hypothesis of this research.

Conflicts of Interest

The authors declare no conflicts of interest regarding the publication of this paper.

References

[1] Musonda, G., Zulu, A. and Lubobya, C.S. (2024) Determination of Total Vector Error of the Phasor Measurement Unit (PMU) Using the Phase Angle Error of a Constant Amplitude Voltage Signal. *Journal of Power and Energy Engineering*, **12**, 34-47. https://doi.org/10.4236/jpee.2024.1211002

[2] Mishra, C., Vanfretti, L., De La Ree, J., Jones, K.D. and Gardner, M.R. (2024) Estimating Clock Synchronization Correction Factor from Synchrophasor Phase Angle Drift. 2024 *International Conference on Smart Grid Synchronized Measurements and Analytics* (*SGSMA*), Washington, 21-23 May 2024, 1-5. https://doi.org/10.1109/sgsma58694.2024.10571449

[3] Almutairy, F., Scekic, L., Matar, M., Elmoudi, R. and Wshah, S. (2023) Detection and Mitigation of GPS Spoofing Attacks on Phasor Measurement Units Using Deep Learning. *International Journal of Electrical Power & Energy Systems*, **151**, Article ID: 109160. https://doi.org/10.1016/j.ijepes.2023.109160

[4] Parvez, I., Sarwat, A.I., Pinto, J., Parvez, Z. and Khandaker, M.A. (2017) A Gossip Algorithm Based Clock Synchronization Scheme for Smart Grid Applications. 2017 *North American Power Symposium* (*NAPS*), Morgantown, 17-19 September 2017, 1-6. https://doi.org/10.1109/naps.2017.8107405

[5] Ravi, A., Saranathan, M., Achuthan, P.H.K., Lavanya, M.C. and Rajini, V. (2022) A Comprehensive Review on the Current Trends in Micro-Phasor Measurement Units. *IOP Conference Series*: *Materials Science and Engineering*, **1258**, Article ID: 012045. https://doi.org/10.1088/1757-899x/1258/1/012045

[6] Mishra, C., Vanfretti, L., Delaree, J. and Jones, K.D. (2024) Internal Clock Errors in Synchrophasor Ambient Data: Effects, Detection, and a Posteriori Estimation-Based Correction. *International Journal of Electrical Power & Energy Systems*, **161**, Article ID: 110208. https://doi.org/10.1016/j.ijepes.2024.110208

[7] Agustoni, M., Castello, P. and Frigo, G. (2022) Phasor Measurement Unit with Digital Inputs: Synchronization and Interoperability Issues. *IEEE Transactions on Instrumentation and Measurement*, **71**, 1-10. https://doi.org/10.1109/tim.2022.3175052

[8] de la O Serna, J.A., Paternina, M.A. and Zamora-Mendez, A. (2021) Assessing Synchrophasor Estimates of an Event Captured by a Phasor Measurement Unit. *IEEE Transactions on Power Delivery*, **36**, 3109-3117. https://doi.org/10.1109/tpwrd.2020.3033755

[9] Rahmati, A. (2016) Accurate Real-Time Measurements of the Smart Grid Phasor Measurement Unit Parameters. *Electric Power Components and Systems*, **44**, 1815-1824. https://doi.org/10.1080/15325008.2015.1114049

[10] Giotopoulos, V. and Korres, G. (2023) Implementation of Phasor Measurement Unit Based on Phase-Locked Loop Techniques: A Comprehensive Review. *Energies*, **16**, Article 5465. https://doi.org/10.3390/en16145465

[11] Ponnala, R., Vijay Babu, P., Leelakrishna, C. and Reddy, R. (2024) Development and Implementation of Synchronized Phasor Measurements for Dynamic State Power System Monitoring and Fault Identification. https://doi.org/10.21203/rs.3.rs-4186838/v1

[12] Kumar, J., Singh, A.K. and Kumar, U. (2023) Effect of WLS Method with Phasor Measurement Unit in State Estimation of Power System. *Journal for Basic Sciences*, **23**, No. 5.

[13] de la O Serna, J.A. (2018) Analyzing Power Oscillating Signals with the O-Splines of

the Discrete Taylor-Fourier Transform. *IEEE Transactions on Power Systems*, **33**, 7087-7095. https://doi.org/10.1109/tpwrs.2018.2832615

[14] Phadke, A.G. and Bi, T.S. (2018) Phasor Measurement Units, WAMS, and Their Applications in Protection and Control of Power Systems. *Journal of Modern Power Systems and Clean Energy*, **6**, 619-629.

[15] Almas, M.S., Vanfretti, L., Singh, R.S. and Margret Jonsdottir, G. (2018) Vulnerability of Synchrophasor-Based WAMPAC Applications' to Time Synchronization Spoofing. 2018 *IEEE Power & Energy Society General Meeting* (*PESGM*), Portland, 5-10 August 2018, 1. https://doi.org/10.1109/pesgm.2018.8586667

[16] Zenati, H., Romain, M., Foo, C., Lecouat, B. and Chandrasekhar, V. (2018) Adversarially Learned Anomaly Detection. 2018 *IEEE International Conference on Data Mining* (*ICDM*), Singapore, 17-20 November 2018, 727-736. https://doi.org/10.1109/icdm.2018.00088

[17] Mohammed, M.Q., Al-Safi, M.G.S. and Faris, A.M. (2024) Statistical Anomaly Detection for Enhanced Cybersecurity Using Ai-Based Wireless Networks. *Ingénierie des systèmes d information*, **29**, 1743-1754. https://doi.org/10.18280/isi.290508

[18] Wang, S.Y., Hijazi, M. and Dehghanian, P. (2023) Smart Measurement Units in Smart Grids: An AI-in-the-Loop Solution for Distributed Intelligence and High-Fidelity Measurements. Association for the Advancement of Artificial Intelligence. https://www.aaai.org

[19] Regev, Y.A., Vassdal, H., Halden, U., Catak, F.O. and Cali, U. (2022) Hybrid AI-Based Anomaly Detection Model using Phasor Measurement Unit Data. arXiv: 2209.12665.

[20] Le, N.T. and Benjapolakul, W. (2018) A Data Imputation Model in Phasor Measurement Units Based on Bagged Averaging of Multiple Linear Regression. *IEEE Access*, **6**, 39324-39333.

[21] Lixia, M., Benigni, A., Flammini, A., Muscas, C., Ponci, F. and Monti, A. (2012) A Software-Only PTP Synchronization for Power System State Estimation with PMUs. *IEEE Transactions on Instrumentation and Measurement*, **61**, 1476-1485. https://doi.org/10.1109/tim.2011.2180973

[22] Bird, J. (2006) Higher Engineering Mathematics. 5th Edition, Khanna Publishers, 699-701.

[23] Ponnala, R., Chakravarthy, M. and Lalitha, S.V.N.L. (2022) Effective Monitoring of Power System with Phasor Measurement Unit and Effective Data Storage System. *Bulletin of Electrical Engineering and Informatics*, **11**, 2471-2478. https://doi.org/10.11591/eei.v11i5.4085

[24] IEEE (2011) IEEE Std C37.118.1-2011; IEEE Standard for Synchrophasor Measurements for Power Systems.

[25] Mohapatra, D. (2015) Development and Hardware Implementation of a Phasor Measurement Unit using Microcontroller. National Institute of Technology, Rourkela, 9-10.

[26] Li, H. (2019) Frequency Estimation and Tracking by Two-Layered Iterative DFT with Re-Sampling in Non-Steady States of Power System. *EURASIP Journal on Wireless Communications and Networking*, **2019**, Article No. 28. https://doi.org/10.1186/s13638-018-1320-1

[27] Chukkaluru, S.L. and Affijulla, S. (2023) Review of Discrete Fourier Transform during Dynamic Phasor Estimation and the Design of Synchrophasor Units. *ECTI Transactions on Electrical Engineering, Electronics, and Communications*, **21**, Article ID: 248548. https://doi.org/10.37936/ecti-eec.2023211.248548

[28] Ali, Z., Saleem, K., Brown, R., Christofides, N. and Dudley, S. (2022) Performance Analysis and Benchmarking of PLL-Driven Phasor Measurement Units for Renewable Energy Systems. *Energies*, **15**, Article 1867. https://doi.org/10.3390/en15051867

[29] Saleem, K., Ali, Z. and Mehran, K. (2021) A Single-Phase Synchronization Technique for Grid-Connected Energy Storage System under Faulty Grid Conditions. *IEEE Transactions on Power Electronics*, **36**, 12019-12032. https://doi.org/10.1109/tpel.2021.3071418

[30] Rao, A.V.K., Soni, K.M., Sinha, S.K. and Nasiruddin, I. (2021) Dynamic Phasor Estimation Using Adaptive Artificial Neural Network. *International Journal of System Assurance Engineering and Management*, **12**, 310-317. https://doi.org/10.1007/s13198-021-01082-2

[31] Islam, A., Bouzerdoum, A. and Belhaouari, S.B. (2024) Bio-Inspired Adaptive Neurons for Dynamic Weighting in Artificial Neural Networks. arXiv: 2412.01454. https://www.researchgate.net/publication/386375425

[32] Nanda, S. and Dash, P.K. (2016) A Gauss-Newton ADALINE for Dynamic Phasor Estimation of Power Signals and Its FPGA Implementation. *IEEE Transactions on Instrumentation and Measurement*, **67**, 45-56.

[33] John, T. (1997) An Introduction to Error Analysis: The Study of Uncertainties in Physical Measurements. University Science Books, 215-217.

[34] Yu, W.P., Yao, W.X., Deng, X.D., Zhao, Y.F. and Liu, Y.L. (2020) Timestamp Shift Detection for Synchrophasor Data Based on Similarity Analysis between Relative Phase Angle and Frequency. *IEEE Transactions on Power Delivery*, **35**, 1588-1591.

[35] Björkhem, F., Myrland, J.B., Jolhammar, T. and Nour, O.M. (2024) Implementation of a Phasor Measurement Unit in Matlab. Department of Electrical Engineering, Uppsala University, 13-17.

[36] Khaledian, E., Pandey, S., Kundu, P. and Srivastava, A.K. (2021) Real-Time Synchrophasor Data Anomaly Detection and Classification Using *isolation Forest*, *Kmeans*, *and Loop*. *IEEE Transactions on Smart Grid*, **12**, 2378-2388. https://doi.org/10.1109/tsg.2020.3046602

[37] (2022) Description of Normal Frequency, The South African Grid Code System Operation Code, Version 10.1. Eskom Transmission Division.